

# Review of ultrafast ion acceleration experiments in laser plasma at Max Born Institute

P.V. NICKLES,<sup>1</sup> S. TER-AVETISYAN,<sup>1</sup> M. SCHNÜRER,<sup>1</sup> T. SOKOLLIK,<sup>1</sup> W. SANDNER,<sup>1</sup>  
J. SCHREIBER,<sup>2</sup> D. HILSCHER,<sup>3</sup> U. JAHNKE,<sup>3</sup> A. ANDREEV,<sup>4</sup> AND V. TIKHONCHUK<sup>5</sup>

<sup>1</sup>Max-Born-Institute, Berlin, Germany

<sup>2</sup>MPI für Quantenoptik, Garching, Germany

<sup>3</sup>Hahn-Meitner-Institute, Berlin, Germany

<sup>4</sup>Vavilov State Optical Institute, St. Petersburg, Russia

<sup>5</sup>CELIA, Université Bordeaux 1, Bordeaux, France

(RECEIVED 31 December 2006; ACCEPTED 26 March 2007)

## Abstract

New perspectives have been opened up in the field of laser–matter interactions due to recent advances in laser technology, leading to laser systems of high contrast and extreme intensity values, where the frontier of maximum intensity is pushed now to about  $10^{22}$  W/cm<sup>2</sup>. Many striking phenomena such as laser-acceleration of electrons up to the GeV level, fast moving ions with kinetic energies of several 10s of MeV, as well as nuclear physics experiments have already actuated a broad variety of theoretical as well as experimental studies. Also highly relativistic effects like laser induced electron-positron pair production are under discussion. All these activities have considerably stimulated the progress in understanding the underlying physical processes and possible applications. This article reviews recent advances in the experimental techniques as well as the associated plasma dynamics studies at relativistic intensities performed at the Max-Born-Institute (MBI). Interactions of a laser pulse at intensities above  $10^{19}$  W/cm<sup>2</sup> with water- and heavy-water droplets, as well as, with thin foils are discussed. Rear and front side acceleration mechanisms, particle dynamics inside the dense target, proton source characteristics, strong modulations in proton and deuteron emission spectra, and finally generation of quasi-monoenergetic deuteron bursts are the topics covered in the article.

**Keywords:** Ion acceleration; Laser plasma; Laser-plasma dynamics

## 1. INTRODUCTION

Recent high intensity laser-plasma interaction experiments have shown unique features such as the acceleration of electrons to energies of 1.2 GeV (Lifshitz, 2006), the acceleration of ions to a few 10s of MeV, and many other phenomena (e.g., see Umstadter, 2003). At present, in spite of extensive studies, the mechanisms of ion acceleration are still a matter of discussion. Ions are created and accelerated either at the rear surface (Snively *et al.*, 2000; Mackinnon *et al.*, 2001; Hegelich *et al.*, 2000, 2002), through the self-consistent electrostatic accelerating field generated by fast electrons escaping in a vacuum (so-called target normal sheath acceleration (TNSA) mechanism), or at the irradiated target front surface (Clark *et al.*, 2000a, 2000b; Maksimchuk *et al.*, 2000). To explain this controversy about the origin

of high-energy ions, Sentoku *et al.* (2002) have proposed the ion acceleration scenario through stochastic heating of electrons, which suggests that for both of these experiments, the origin of the ions is the same and that the only difference is in the plasma thickness: whether or not the plasma extends to the rear surface. Particle-in-cell (PIC) simulation studies of the proton acceleration at both front and rear sides of the target (Sentoku *et al.*, 2003), have shown that at the laser-irradiated target surface, the laser pressure sets an electric field, which sweeps electrons from the interaction region, and induces front-surface acceleration (FSA) of ions into and through the target. Here, the laser intensity, pulse length, and target thickness are playing a decisive role.

PIC Simulations suggest a variety of mechanisms that may be responsible for acceleration at the front surface: formation of multiple collisionless electrostatic shocks at high plasma density (Denavit, 1992; Silva *et al.*, 2004; Wei *et al.*, 2004), a solitary wave produced by shock-wave decay in a plasma slab irradiated by an intense picosecond laser pulse

Address correspondence and reprint requests to: S. Ter-Avetisyan, Max-Born-Institut, Max-Born-Str. 2a, Berlin D12489, Germany. E-mail: sargsis@mbi-berlin.de

(Zhidkov *et al.*, 2002), or a mechanism wherein the ponderomotive pressure of the short laser pulse displaces the background electrons, and the ions are accelerated by the electrostatic field of the propagating double layer (Shorokhov & Pukhov, 2004).

Up to now, it is not clear which process, rear or front surface acceleration, is dominant. Since unambiguous experimental observations by different groups explained by invoking different acceleration scenarios, it is likely that specific experimental conditions used in different experiments, such as laser pulse duration, pulse shape/contrast, or target properties play a fundamental role. PIC simulations (Wilks *et al.*, 2001; Pukhov, 2001) and observations (Zepf *et al.*, 2003; Karsch *et al.*, 2003) show that ions can be produced at the front and the rear sides simultaneously, even if the generation processes are quite different.

In this paper, we discuss peculiarities of the ion acceleration from the rear and front sides of thin foil targets, irradiated by ultrashort (sub 50 fs) high intensity ( $\sim 10^{19}$  Wcm<sup>-2</sup>) laser pulses. Space charge displacement due to resonance absorption and the action of the laser ponderomotive force on the electrons are leading processes. The investigations showed that the laser pulse contrast plays a fundamental role for the interaction (Kaluza *et al.*, 2004; Ter-Avetisyan & Nickles, 2006). This is, to our knowledge, the first observation of ions accelerated from the front and the backsides of thin foil target, where the difference of their origin were selected by emission direction, which is coupled to different acceleration scenarios. Under these circumstances, the entire ion acceleration scenario can be controlled. A simple geometry of laser-target interaction is used to elucidate the particle acceleration dynamics.

Another important point is the dynamics of the plasma development and the ion acceleration. The latter is crucial for the understanding and possible controlling the acceleration processes. The ions are produced either with a very broad instantaneous energy (velocity) spread during a very short time period, or the ion energy is a function of time and the instantaneous energy (velocity) spread is relatively small. Therefore, time-resolved measurements are required to learn more about the acceleration dynamics in the plasma, e.g., which ions are accelerated first, and what in turn, is their influence on the acceleration of the other ion species (Hegelich *et al.*, 2002). In order to record the emitted high-energy ions temporally resolved in dependence on both their charge states and energies, we have developed a diagnostic (Ter-Avetisyan *et al.*, 2005b) consisting of a modified Thomson-parabola spectrometer. For this purpose, a pulsed electric field as an under damped harmonic oscillation was applied to the deflecting plates in the Thomson spectrometer. As a result, the trajectories did not only reveal the energies of the particles due to their deflection in the magnetic field, but also their temporal evolution according to the applied electric pulse shape. The applied time delay between the plasma creation and the applied electric field should be the sum of the acceleration time in the plasma

sheath and the time of flight (TOF) of the ions. The last one can be calculated from the ion energies measured in the spectrometer because the geometry of the experiment is known. The temporal relation between the applied electric pulse shape and the delay, as well as the measured modulated ion spectrum, and the TOF will characterize the temporal evolution of the ion acceleration.

Laser energy transfer to the target, electron transport, ion generation, and acceleration processes are complex phenomena, which are governed by the target internal electric and magnetic fields. The measurement of these fields is one essential prerequisite for the further understanding of energy transport and energy conversion triggered by laser fields of relativistic strength. Protons with energies of several MeV up to 10s of MeV have already been used to trace strong electric and magnetic fields in laser produced dense plasmas, in preliminary demonstration experiments (Borghesi *et al.*, 2001). The beamlike characteristics of the generated ions, such as high collimation, high particle flux, and short pulse duration have been demonstrated, making them attractive for new applications. Recently Cowan *et al.* (2004), and Borghesi *et al.* (2004) reported on laser accelerated proton beams with very low emittance values of  $\sim 10^{-3}$  mm mrad and  $\sim 10^{-1}$  mm mrad, respectively. These features in combination with the spatial stability of the source are the principle requirements for using these beams in radiographic imaging experiments. However, small fluctuations in the acceleration sheath could change the position of the proton source on the rear side of the laser-irradiated target. An observation of these small fluctuations has become possible with a Thomson spectrometer combined with a high spatial resolution (Schreiber *et al.*, 2006). Thereby we analyze the beam spatial fluctuations and the partial divergence of protons emitted off thin aluminum foils. Thus, we obtained not only additional properties of the angular or spatial emission of the source, but also aspects of its temporal evolution can be discussed.

Also, it turns out that almost all perspective applications in laser-driven ion acceleration depend on the production of nearly monoenergetic proton and ion bunches with high beam quality and reliability. In particular, post-acceleration, and beam transport in new compact MeV accelerators (Habs *et al.*, 2001) would greatly benefit from a monoenergetic spectrum; imaging radiography (Cobble *et al.*, 2002; Borghesi *et al.*, 2002, 2005) can be improved in terms of resolution and contrast. In contrast to laser acceleration of electrons, however, the experimental results on laser acceleration of ions over the last few years have only exhibited broad energy spectra. Recently Hegelich *et al.* (2006) and Schwoerer *et al.* (2006) have reported on the experimental observations of ion and proton emission, correspondingly, in a narrow energy band. There is also a proposal for GeV laser-ion acceleration made by Yin *et al.* (2006). Here, we report on the laser acceleration of deuterons from a special target system (heavy-water droplets) with ultra-short, ultra-intense laser pulses, leading to the observation of a rather

sharp peak in the energy spectrum (Ter-Avetisyan *et al.*, 2006). The results can be explained by a simple physical model related to the spatial separation of two ion species resulting from a high contrast laser pulse excitation of a finite-volume target. Recently Albright *et al.* (2006) have developed an analytic model that predicts the mean energy and quality of monoenergetic ion beams with substrate material and light-ion layer composition and thickness.

## 2. EXPERIMENT

In the experiments, thin foils or droplet targets were irradiated by  $\leq 50$  fs, 700 mJ Ti: Sapphire laser pulses (Kalachnikov *et al.*, 2002). With an  $f/2.5$  off-axis parabolic mirror, a maximum vacuum intensity of  $(1-2) \times 10^{19}$  W/cm<sup>2</sup> was reached. The temporal contrast of the laser pulse was characterized by a scanning third order cross correlator with a dynamic range of  $10^{10}$ , having a temporal resolution of 150 fs, and a scanning range of  $\pm 200$  ps. The pulse shape several ns before main pulse was controlled by a fast

photodiode with a temporal resolution of about 300 ps. In typical operating conditions, the amplified spontaneous emission (ASE) pedestal of the laser pulse in a temporal window of several picoseconds before the pulse peak had a relative size of about  $5 \times 10^{-7}$ . Driving the amplifier of the Ti: Sapphire laser with specifically delayed pump mode could reduce the ASE pedestal. This led to a reduction of output pulse energy up to 550 mJ, but to an improvement of the ASE level down to  $10^{-8}$ . The pulse shape close to the peak was unchanged, and in both cases, no pre-pulses preceding the main pulse were observed.

Measurements of the ion energies were carried out with a Thomson parabola spectrometer, where the ions were detected by 40 mm diameter multi-channel plate (MCP) detector coupled to a phosphor screen, and a Charge-Coupled-Device (CCD) camera. The whole system is absolutely calibrated and enables single-particle detection (for further details, see Ter-Avetisyan *et al.*, 2005b). The background pressure in the experimental chamber was a few times  $10^{-6}$  mbar and in the spectrometer even lower. This sensitive detection setup makes it possible to measure in one single laser shot the ion spectrum in absolute terms. At the detector plane perpendicular to the ion propagation direction, the energy spectra of different ion species are detected along different parabolas as visualized in Figure 1a for the spectra from heavy water droplet target. Evaluated spectra from these traces are depicted in Figure 1b. For emission direction resolving measurements, three Thomson spectrometers with an acceptance angle of 256 nsr were positioned around the target at  $0^\circ$ ,  $45^\circ$ , and  $135^\circ$  to the laser propagation direction. Spatial and energy distributions of the ions were measured for normal and  $45^\circ$  laser irradiance of the target.

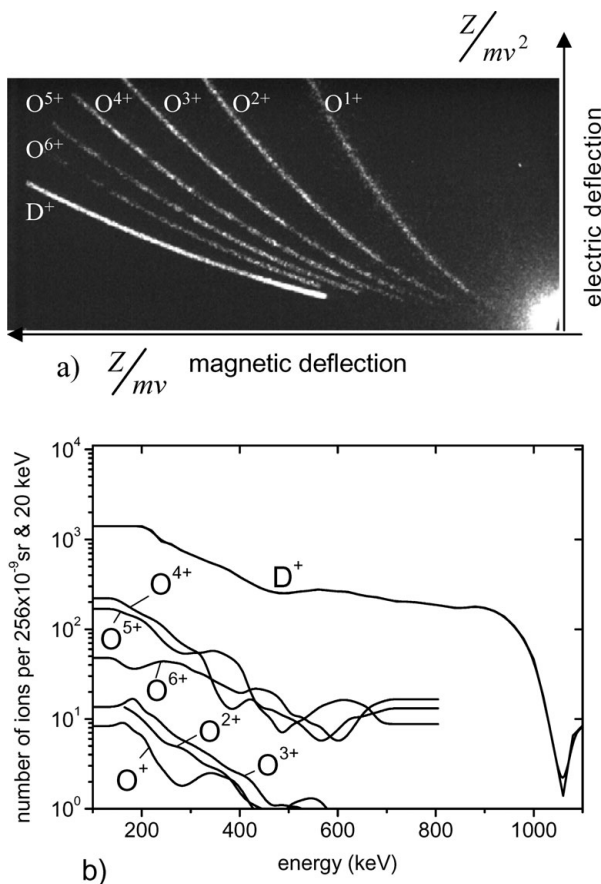


**Fig. 1.** (a) Image from the MCP-phosphorous screen of an emitted ion spectrum from a heavy water droplet taken from a single laser shot in backward ( $135^\circ$  to laser propagation) direction (right blob – “zero” point: radiation impact along spectrometer axis, Z-ion charge state, m-ion mass, v-ion velocity). (b) Evaluated ion emission spectra. The fall of the oxygen ion numbers for charge states 4, 5, and 6 at higher energies is blended by the “zero” point signal. The deuteron cut off energy is around 1 MeV.

## 3. ION ACCELERATION FROM FRONT OR REAR TARGET SURFACE

The absorption mechanisms of intense laser radiation at the target are the basic processes in laser-matter interaction. Inverse bremsstrahlung and resonance absorption are very familiar. Whereas inverse bremsstrahlung has a maximum absorption when the irradiation is normal to the target plane, resonance absorption can drive efficiently electrons to high energies at non-normal angles of laser incidence. These electrons create a smooth density and temperature profile in the interior region of the target, with a maximum in a direction normal to the target.

At high-intensity laser irradiation, the ponderomotive force (Wilks *et al.*, 1992; Lefebvre & Bonnaud, 1997; Kruer & Estabrook, 1985) starts to play a decisive role. In contrast to inverse bremsstrahlung and resonance absorption, which causes the quiver motion of the electrons in the oscillating field of the laser, the ponderomotive force accelerates the electrons in the laser propagation direction if the laser intensity gradient is high enough; e.g., if the laser pulse length is shorter than its focal spot diameter. The ponderomotive force drives the electrons with a step- or plateau-like

density profile, and has a strong directionality along the laser propagation direction. The laser energy transfer to the hot electrons could also be carried by fast plasma waves through the nonlinear ponderomotive force (Tajima & Dawson, 1979) and by the laser field itself (Pukhov *et al.*, 1999). These mechanisms are not mutually exclusive. Their relative contributions depend strongly on the particular target and laser parameters, and could give a contribution to the generation of electrons and, in turn, to ion acceleration mechanisms.

In experiments by Stein *et al.* (2004), irradiating planar targets with intense 100 fs laser pulses at angles less than  $45^\circ$  to the normal, it was shown that indeed two groups of separately located hot electron populations were present at the target rear side. The authors attribute that to the electrons resulting from resonance absorption ( $e_R^-$  in Fig. 2) propagating in the target normal direction whereas; the ponderomotively-accelerated electrons ( $e_p^-$  in Fig. 2) propagate in the laser irradiation direction. In terms of ion acceleration, it is obvious that both electron populations at the target rear side would create electrostatic fields that accelerate ions/protons according to so-called target normal sheath acceleration (TNSA) mechanism (Clark *et al.*, 2000a, 2000b). This means that, at the target rear surface, one also has two sources from which the ions are accelerated (Fig. 2). The acceleration direction of ions from the rear side is normal to the target, while ions from the front side of the target could be accelerated also in the direction of the ponderomotively driven electrons. Those ions propagate through the target, leaving the target rear surface in the laser propagation direction. Therefore, one can expect ion emission in two directions: either in the laser propagation direction due to ponderomotively driven electrons, or normal to the surface due to electrons driven by resonance absorption, depending

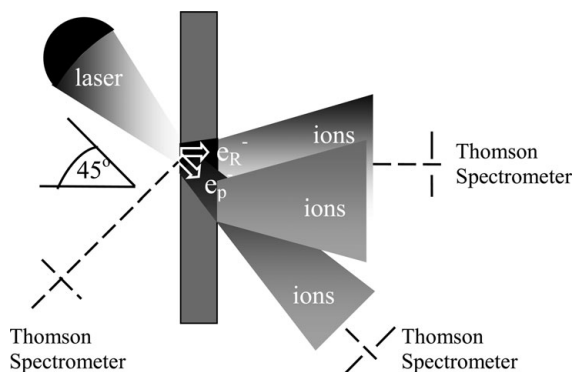


**Fig. 2.** Schematic of the experiment, showing two ion beams accelerated due to the hot electron populations created by resonance absorption ( $e_R^-$ ) and ponderomotive acceleration ( $e_p^-$ ) directed normal to the target surface and in the laser irradiation direction, respectively. Both electron populations at the target rear side would create electrostatic fields separated in space that could accelerate the ions. The ions from the rear side will be accelerated in the direction of the target normal, whereas the ions from the front side are accelerated not only in the target normal direction due to ( $e_R^-$ ) electrons, but they could also be accelerated in the direction of the ponderomotive electrons ( $e_p^-$ ); that is, in the direction of laser propagation.

on which laser energy absorption mechanism is dominant. If both mechanisms are equivalent, one could observe a widely spread proton emission as described by Fuchs *et al.* (2005). Therefore, measuring the angle-resolved ion emission as well as spatially resolved ion source characteristics under conditions where the laser energy absorption mechanisms are well defined, one could clarify whether the ions come from the front or rear surface of the target.

In our experiments, thin (20  $\mu\text{m}$ ) planar Mylar foil targets were irradiated with a “high” ( $10^{-8}$ ) and “low” ( $5 \times 10^{-7}$ ) laser pulse contrast with a pulse peak intensity of  $1.2 \times 10^{19} \text{ W/cm}^2$  (Ter-Avetisyan & Nickles, 2006). At normal laser incidence on the target and with an improved laser pulse contrast of up to  $10^{-8}$ , an ion spectrum was registered only in the target normal direction. Ions were emitted neither at  $45^\circ$  (in contrast to Fuchs *et al.*, 2005) nor at  $135^\circ$  to the target normal. In this interaction geometry, it is obvious that the hot electrons, no matter how they are created, will build up the acceleration field at the target rear side. This in turn accelerates the ions either from the front or rear side of the target only in a direction normal to the target. This result is in agreement with (Clark *et al.*, 2000a, 2000b) and many others, which have reported ion emission at an angle within  $15^\circ$ – $20^\circ$ . In the spectrum, one can identify protons, carbon ions from  $\text{C}^{1+}$  up to  $\text{C}^{4+}$ , and weak  $\text{C}^{5+}$  ion signals.

When the target was turned to  $45^\circ$  with respect to the laser incidence, we measured in the direction of laser propagation only protons and  $\text{C}^{4+}$  ions (Fig. 3). Following the arguments by Ter-Avetisyan and Nickles (2006), the ions emitted in the laser propagation direction should stem only from the front surface (Fig. 2), accelerated by the ponderomotively driven electron population from the front surface. Additionally, according to our supposition above, one could also expect two ion sources at the rear side of the target emitting ions normal to the target (Fig. 2). In order to prove this, we performed an energy-dispersed pinhole imaging of the source (for more details cf. Section 4). The source at the target rear surface was imaged with high magnification on a MCP detector plate by placing the entrance pinhole of the Thomson spectrometer (with a diameter of 30  $\mu\text{m}$ ) at a distance of 5 cm from the source. This made it possible to image the ion source with a 15 times magnification, and simultaneously to record the ion energy distribution (for further details, see Schreiber *et al.* (2006)). The two parallel proton traces measured in the direction normal to the target surface (Fig. 4) are indicative of two separate proton sources. Figure 4 also shows that the parabolas are not perfect. This coincides with our findings (Schreiber *et al.*, 2006 see Sec. 5) that the source position for protons is variable. Notice that the two parallel traces in Figure 4 are changing in a similar manner, which indicates a complex source dynamics.

The second source (or second proton trace) appeared only when protons were measured in the laser propagation direction. It is worth noting that  $\text{C}^{4+}$  ions measured in the laser direction are of the highest charge state that can be ionized

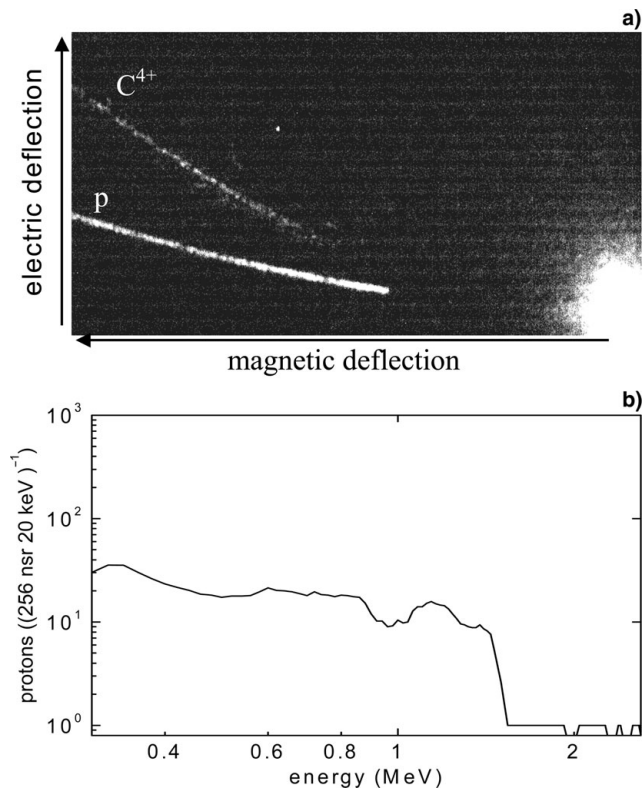


**Fig. 3.** (a) CCD picture of accelerated ion spectra; and (b) deduced proton spectra at  $45^\circ$  laser incidence on the target measured in the direction of laser propagation. Here  $C^{4+}$  ions and the proton signal could be identified. There is no signal from low charge states of carbon ions.

(Ammosov *et al.*, 1986) at the laser intensities used, and which could then undergo an acceleration process. This is in good agreement with a model calculation given in Hegelich *et al.* (2002), that all carbon ions are sequentially ionized up to  $C^{4+}$ . This picture is a particular characteristic of highly contrasted laser pulses. Additionally, the protons from the front side have a plateau-like spectrum with a sharp cut off (Fig. 3). This is consistent with predictions of PIC simulations (Silva *et al.*, 2004; Wei *et al.*, 2004), that

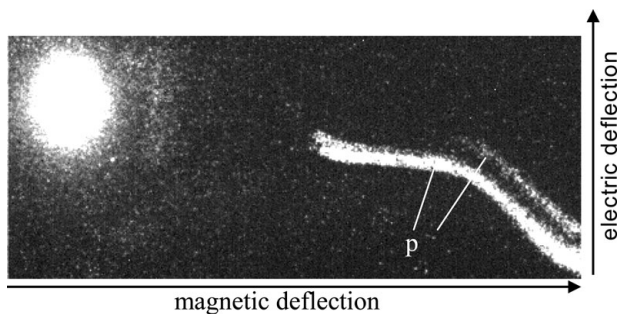


**Fig. 4.** CCD picture of the proton spectrum at  $45^\circ$  laser incidence on the target measured in the direction of the target normal. Two parallel proton parabolas show the existence of the two sources of proton emission. Figure shows that the parabolas are not perfect. This coincides with our previous findings (Sec. 5) that the source position for protons is variable.

the interaction of collisionless electrostatic shocks formed at the front surface are responsible for the observed plateau structure in the ion spectrum, and that the plateau provides a direct signature for shock acceleration at the front surface of the target.

In contrast to that, at the same  $45^\circ$  laser to target normal irradiation, but at a reduced laser pulse contrast with a “typical” level of  $5 \times 10^{-7}$ , no ions or protons were registered in the laser direction, and no second ion source was observed. These observations are consistent with a picture of the interaction where laser energy absorption is dominated by resonance absorption. Figure 5 shows the emitted ion spectra in the direction normal to the target at four successively increased laser intensities (from Figs. 5a to 5d). An increase of laser pulse intensity (Fig. 5) is accompanied by a growth of the mean ion charge states. First, at the intensity of  $2 \times 10^{18}$  W/cm<sup>2</sup> we have ions  $C^{1+}$ ,  $C^{2+}$ , and  $C^{3+}$  (Fig. 5a), then at  $3 \times 10^{18}$  W/cm<sup>2</sup> –  $C^{2+}$ ,  $C^{3+}$ , and  $C^{4+}$  (Fig. 5b), at  $5 \times 10^{18}$  W/cm<sup>2</sup> –  $C^{4+}$ , (Fig. 5c), and finally, when the laser intensity is about  $10^{19}$  W/cm<sup>2</sup>, only protons are detected and no more carbon ions could be recorded (Fig. 5d). That means that the number of carbon ions has dramatically decreased a recedes below the detection limit of the experimental setup (acceptance angle of the Thomson spectrometer is 256 nsr), while the laser intensity was increased only by a factor of two.

An increase of ions charge state ( $Z$ ) with an increase of laser intensity (Figs. 5a, 5b, 5c) could be understood as an increase of the acceleration field, which shows also increased cut off energy of the protons. But with an increase of average ion charge state, Coulomb force in the ion beam starting to play a decisive role. An ambipolar acceleration force increases linearly with an ions charge state ( $\sim Z$ ), while Coulomb repulsion increases as  $\sim Z^2$ . Therefore, the ion beam before being accelerated or during the acceleration process could explode. Coulomb explosion takes place homogeneously into  $4\pi$  and the number of ions in the detection solid angle decreases by at least two orders of magnitude, which is already below the detection limit of the setup (Fig. 5d). As a result, pure proton beam is detected.

This is an important feature of short pulse and high intensity laser-plasma interaction, when the sharp increase of accelerating field sharply increases the ion charge state, and as a result, the ions explode. In contrast to that, at relatively long laser pulse interactions (Hegelich *et al.*, 2006; Brambrink *et al.*, 2006b), more smooth increase of the accelerating potential takes place, and the charge accumulation effect could be avoided. Additionally, Brambrink *et al.* (2006b) have shown that the ion front divergence is 1.6 times smaller than that of the protons, therefore, the proton front could not be affected by accumulated charge, which we see also in the experiments, and the rear side target structures could be detected (Brambrink *et al.*, 2006a).

It is worth noting that no ion emission was observed at  $135^\circ$  in any case. Additionally, in contrast to the protons from the front side, which have a plateau-like spectrum

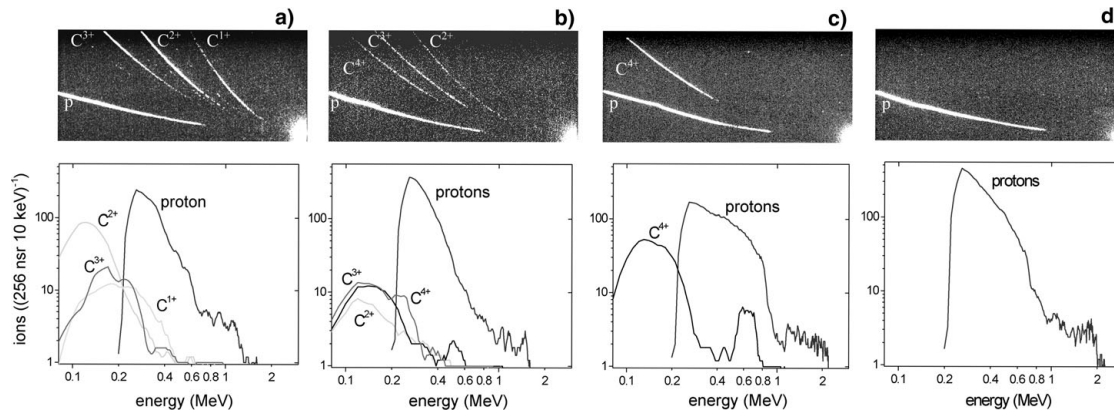


**Fig. 5.** At a laser pulse contrast level of  $5 \times 10^{-7}$ , the emitted ion spectra measured in the direction of the target normal at  $45^\circ$  laser incidence on the target for four successively increasing laser intensities: (a)  $2 \times 10^{18}$  W/cm<sup>2</sup>; (b)  $3 \times 10^{18}$  W/cm<sup>2</sup>; (c)  $5 \times 10^{18}$  W/cm<sup>2</sup>; and (d)  $10 \times 10^{18}$  W/cm<sup>2</sup> are shown. On the top the CCD pictures of the ion spectra, and on the bottom the corresponding evaluated spectra are shown.

with a sharp cut off energy (Fig. 3), the proton spectrum from the rear side (Fig. 5) shows a rapidly decreasing distribution.

#### 4. TIME RESOLVED PARTICLE DIAGNOSTICS

For investigations of the particle acceleration from high-intensity laser plasmas very often Thomson mass spectrometers are used, which have both a high enough resolution to resolve the energy and charge states of the ions, and enough sensitivity to allow absolute measurements also in a single laser shot. However, those records contain only information about ion energies that were finally accumulated during the acceleration process, but no information about the dynamics of the plasma development, and the ion acceleration. The latter is crucial for the understanding and possible controlling the acceleration processes. Therefore, time-resolved measurements are required to learn more about the acceleration dynamics in the plasma, e.g., which ions are accelerated first, and what in turn, is their influence on the acceleration of the other ion species (Hegelich *et al.*, 2002).

In the spectrometer, a pulsed electric field was created by the voltage having a shape of an under damped harmonic oscillation and a tuneable delay relative to the laser pulse (Ter-Avetisyan *et al.*, 2005b). This oscillating electric field modulates the trajectories of the ions when they propagate through the spectrometer, in a similar way, as if their traveling time in the deflecting plates is shorter than the half period of the applied electric field. Additionally, at different time delays, different parts of the ion energy spectra will be modulated. The applied time delay ( $\Delta T$ ) between the laser pulse and the electric pulse is the sum of the time from the moment when the ion was “born” ( $t_0$ ), and the traveling time up to the electric plates of the spectrometer ( $l/v$ ):  $\Delta T = t_0 + l/v$ . With the measured ion energy or velocity ( $v$ ) as well as with the known traveling distance ( $l = 48.4 \pm 0.1$  cm), the arrival time ( $l/v$ ) of the ion in the spectrometer can be determined. Then one can evaluate the time

( $t_0$ ), that is necessary for different ion species to be accelerated. Several such “snapshots” are presented in Figure 6, with time delays of (a) 66.8 ns, (b) 142 ns, and (c) 182 ns. Here a heavy water droplet is used as a target. In Figure 6, a bright spot on the left is formed by energetic photons moving along the axis of spectrometer. The ions and protons, which are reaching the spectrometer before or after applied deflecting voltage pulse, form a bright horizontal line in all images in Figure 6. At first, the deuterons are arriving at the spectrometer (Fig. 6a), and only they are deflected in the pulsed electric field applied with the delay of 66.8 ns corresponding to the time-of-flight (TOF) of deuterons. All other ions are dispersed by the magnetic field of spectrometer, but they are overlapped in the bright line of the images. Then, at the delay of 142 ns, the oxygen ions with the deuterons are deflected (Fig. 6b). At the larger time delay only oxygen ions can be seen (Fig. 6c).

The time resolution is calculated by  $\Delta t = (\Delta l/l + \Delta v/v) \cdot l/v$ . If the relative error of the measured ion velocity is not more than  $\Delta v/v \approx 1\%$ , which is mainly defined by the geometry of the detection system, and if the accuracy of the distance measurement is  $\Delta l \approx 0.1$  cm, then the time resolution of the system can be estimated as:  $\Delta t \leq 0.01 \cdot l/v$ . For our setup, the time resolution of the high-energy end (cut off) of the measured ion spectra (around 1 MeV for deuterons) would be  $\Delta t \leq (4 - 5) \cdot 10^{-10}$  s. It is obvious that the time resolution of the setup could be improved by increasing the accuracy of the ion velocity measurement. This could be done by both an increased dispersion of the spectrometer and a reduction of the distance between the spectrometer and the source while keeping the relative distance accuracy. Thus, an increased signal at the detector additionally would allow one to reduce the entrance pinhole diameter of the spectrometer. The latter helps further to increase the resolution. Practically, the time resolution could be improved up to a ps-level.

However, already the time resolution of  $\Delta t \leq (4 - 5) \cdot 10^{-10}$  s could be sufficient to investigate the ion acceleration

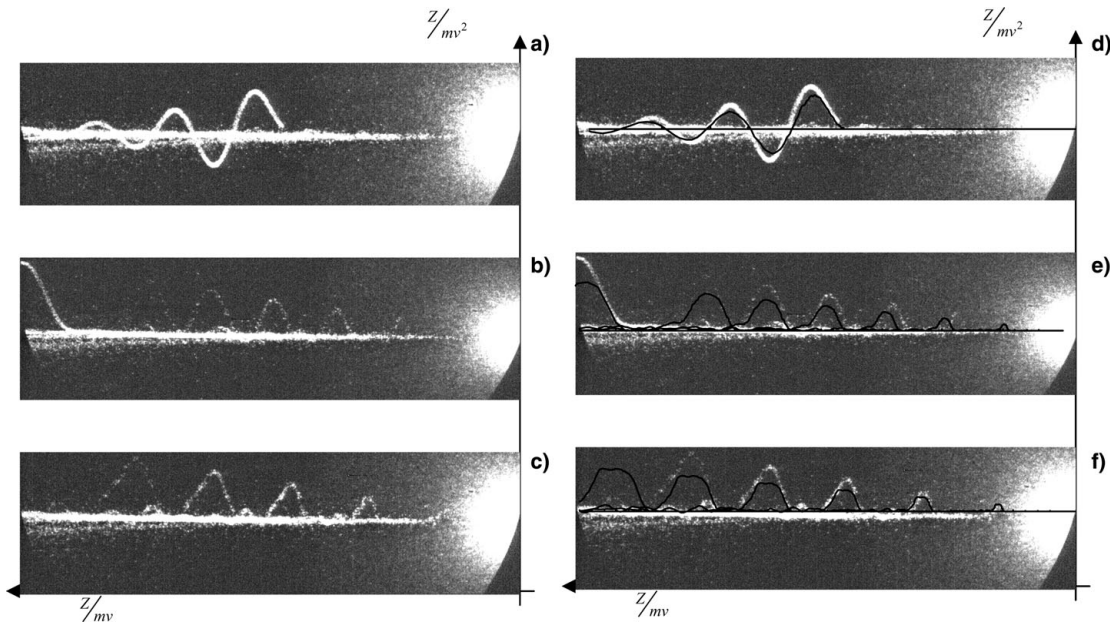


**Fig. 6.** Images of deflected ion traces by the modulated electric field as a function of the ion velocity and their respective arrival time in the spectrometer: The deuterons show clearly the shape of the electric field which is applied to the field plates of the spectrometer with a delay of (a)  $\Delta T = 66.8$  ns, (b) 145 ns, (c) 182 ns to the laser pulse. Oxygen-ions appear definitely later at (b) 145 ns and (c) 182 ns to the laser pulse and show mainly one bump for each ion species. (From left to right: remaining deuterons in (b) and  $O^{2+}$ ,  $O^{3+}$ ,  $O^{4+}$ ,  $O^{5+}$ ,  $O^{6+}$  are subsequently visible). In (d), (e), and (f) these snapshots of the ions from (a), (b), and (c) are shown in comparison with simulated spectra, correspondingly, when all ions start at the same instant.

dynamics in a laser plasma source. With the assumption of simultaneous ion acceleration, the simulated spectra are shown in Figures 6d, 6e, and 6f. They correspond to the measured spectra 6a, 6b, and 6c. The calculations are in good agreement with the experimental results and clearly reproduce the shape of the measured ion spectra. This shows the proof of principle and allows one to interpret the temporal scenario of the ion emission under our experimental conditions as follows: The deuterons and oxygen ions are accelerated simultaneously and are delayed on the way to the spectrometer only due to their velocity difference, which is measured via the difference in the arrival times at the detector.

## 5. ENERGY-DISPERSED PINHOLE IMAGING OF THE PROTON SOURCE

Here we analyze the spatial stability and the partial divergence of protons emitted from thin aluminum foils as a function of their energy. Thus we obtain not only additional properties of the angular or spatial emission of the source but also address some aspects of its temporal evolution.

In previous studies (Busch *et al.*, 2003; Ter-Avetisyan *et al.*, 2004, 2005a, 2005b) we used the Thomson spectrometer in a 1:1 imaging mode: an entrance aperture of 200 micron in diameter was located at a distance of 30 cm from the ion source under investigation. The imaging plane of the ion traces was also at a distance of 30 cm behind the aperture. Laser irradiated tiny water droplets (Busch *et al.*,

2003; Ter-Avetisyan *et al.*, 2005b) produced perfect parabolic traces from all registered ions. This demonstrates that the magnetic and electric field geometry inside the spectrometer produces no artefacts in the ion trajectories. In experiments with planar target foils however, kinks or small bumps in ion traces became visible when strong ion, mainly proton, emission occurred.

In order to study the phenomenon in detail, we set up a Thomson spectrometer in a 1:15 imaging mode: A 30  $\mu\text{m}$  pinhole is at a distance of 5 cm from the source and the detector screen location is 75 cm behind the pinhole. The electric and magnetic fields were placed 14 cm in front of the detector screen. With this disposition we can look at an area on the target rear side with an extension of  $\pm 400 \mu\text{m}$  with respect to target centre with a resolution of about 30 micron.

An example of recorded proton emission spectra from 13  $\mu\text{m}$  aluminum foil target with magnification of 1:15 is

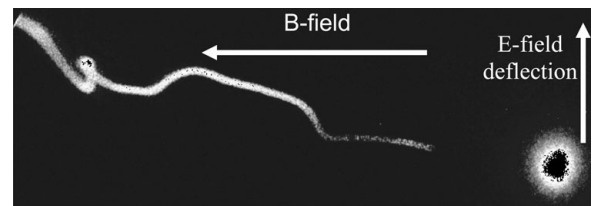


**Fig. 7.** Photograph of an energy dispersed proton trace, which is detected with a multichannel plate and phosphorous screen imaging device and a pinhole Thomson spectrometer. The proton trace detected with a magnified imaging ratio of 1:15.

depicted in Figure 7. The occurrence of such a wiggled trace is reproducible. The explicit shape varies from shot to shot while similarities between adjacent shots are clearly visible. The high energy part of the emission between the cut off and about 50% of the cut off energy obeys the expected ideal parabolic trace. The observed phenomenon is a property of the emitting proton source and it is not due to a possible injection of additional charged particles into the spectrometer. This has been verified by either putting an additional aperture at a 4 kV potential in front of the spectrometer entrance and/or switching a grounded short-circuit to the electrical field plates. Our apparatus is a combination between a pinhole camera and a spectrometer.

The fact that we detect non-blurred, although wiggled, parabola traces confirms a small normalized emittance (transversal temperature) of proton beams ( $<0.01$  mm mrad) demonstrated by Cowan *et al.* (2004). In our setup, the whole beam illuminates the pinhole and we detect a trace with a certain spread. This spread is a measure of the divergence of the small beamlet cut out by the pinhole. We call it the partial beam divergence. The position of the trace at the detector is determined by the emission coordinate from the target surface as well as by the energy of the ions. The latter determines the deflection angle inside the spectrometer. Three parameters define the particle orbit. There are the two angle coordinates (we call them the target emission coordinates); and the emission from the virtual target point that produces an ideal undisturbed Thomson parabola trace crossing the registered “zero” point at the detector plane.

Figure 8 shows the result of reconstruction of the emission source position using the measured traces shown in Figure 7 (cf. details in Schreiber *et al.*, 2006). The changes in the target emission coordinates and the decrease of the partial beam divergence with increasing proton energy are shown. The partial beam divergence values, one can calculate from the present geometry (distance of the source to the detector), and trace the spread. A beam analysis across the whole beam would require an array of pinholes, the so-called pepperpot, which gives a possibility to determine the beam emittance. However, from derived numbers, one can give an estimate of the lower limit of the beam emittance as  $(2-3) \times 10^{-3}$  mm mrad for (2–3) MeV proton energy, and about  $10^{-2}$  mm mrad for (0.2–0.3) MeV proton energy. These values show that the proton beam is well suited for application in imaging experiments.

## 6. FUSION NEUTRONS REVEAL EXPLOSION CHARACTERISTIC OF DROPLETS

The ion emission from high intensity laser irradiated targets can be measured directly while the ion dynamics inside the dense targets is difficult to access. Under these circumstances, the fusion neutron spectroscopy has been shown (Habara *et al.*, 2003; Hilscher *et al.*, 2001) to be a powerful tool, because neutrons produced in fusion reactions penetrate

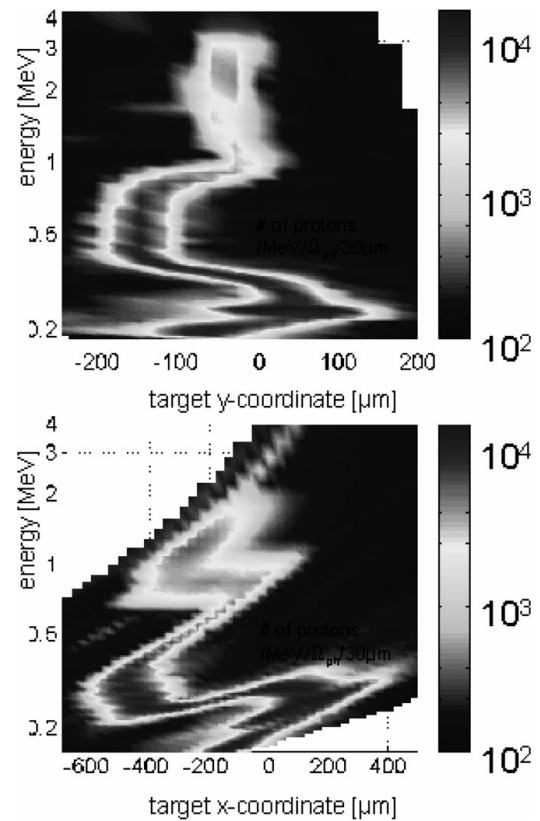


**Fig. 8.** Result of the analysis of the recorded proton emission shown in Figure 7. The source emission coordinates  $x$  and  $y$  are plotted as a function of proton energy.

dense matter almost undisturbed, while their energies reflect the ion kinematics inside a target.

Additionally, laser driven neutron sources could be established with the 2.45 MeV D(d,n)-fusion neutrons with a pulse within  $\sim 5$  ps in the near vicinity of a 100-micron extended source. The advantage of such a neutron source relies on a relatively low laser energy input of a few hundred mJ. Given sufficient flux, such a neutron pulse can be used to expose a piece of solid matter, where, due to the energetic neutron impact, a change in its structure takes place.

In our experiments, four neutron detectors were positioned at observation angles of  $0^\circ$ ,  $135^\circ$ ,  $90^\circ$ , and  $45^\circ$  relative to the laser beam at distances between 322 and 349 cm, viewing the target through 2 mm aluminum windows for neutron TOF measurements. The detectors consist of a liquid scintillator (NE213) with a diameter of 12.7 cm, and a thickness of either 2.54 cm or 5.08 cm, which is coupled to a 4 inch photomultiplier tube. Directly in front of each scintillator a 6 cm thick lead brick wall was positioned in order to reduce the amplitude of the prompt  $\gamma$ -pulse. On-line measured thresholds for the neutron detection were used to calculate the detector efficiencies (more details cf. Schnürer *et al.*, 2005)). As with heavy-water targets, a single droplet within a train of droplets and newly developed pulsed water-spray have been used (Ter-Avetisyan *et al.*, 2003). A single droplet has a diameter of about 20  $\mu\text{m}$

(Hemberg *et al.*, 2000) and a droplet-separation in the train of 70  $\mu\text{m}$  (centre to centre). Detailed characterization of the spray gave a number density of droplets near the nozzle of  $10^{11}$  droplets/ $\text{cm}^3$  with a droplet diameter of 0.15  $\mu\text{m}$ . The mean atomic density 1 mm below the nozzle where the laser is focused is  $>10^{18}$  atoms/ $\text{cm}^3$ . In a Rayleigh-range of 70  $\mu\text{m} \times 2w_0 = 6 \mu\text{m}$  about 200 micro-spheres are exposed to the focused laser radiation. In the following results on single droplet targets as well as spray targets are described.

### 6.1. Single droplet target

In respect to the spherical symmetry of the target and the observed angular particle emission characteristics in our experiment (Busch *et al.*, 2003), we define the inward and outward accelerated deuterons from the droplet. In order to infer data for the inward accelerated deuterons, which should be responsible for neutron generation, a careful analysis of the whole target system is indispensable. A closer look at the target system itself reveals that the neighbor droplets in the train of droplets cannot be neglected. Thus, in our system, we have always two secondary droplet targets, one above and one below the target droplet, which are seen by the target droplet with a solid angle of about  $2 \times 90$  msr.

The quantification of different neutron sources in the experiment requires a careful calibration of the whole detector arrangement (cf. details in Schnürer *et al.*, 2004). The uncertainties of the neutron detection efficiencies of all four detectors and neutron background were measured. The scattering of 2.5 MeV neutrons from structures in the MBI target room area was calculated with the FLUKA-code (2002).

The neutrons have an isotropic angular emission profile. Only a small amount is produced inside the exploding droplet, while a significant number of neutrons are produced from secondary droplet targets by direct bombardment of the radially ejected deuterons. Additionally, it appears that the neutrons in the forward direction ( $0^\circ$ ) are more energetic than those in the backward direction ( $135^\circ$ ) (in Figs. 9a and 9b correspondingly), which indicates that these neutrons must have been produced inside the target droplet by energetic deuterons preferentially moving in the forward direction. This finding is corroborated by the observation that the energy deviations are almost symmetric to 2.45 MeV: about +300 keV at  $0^\circ$  and -200 keV at  $135^\circ$ . This finding is very similar to the reported (Hilscher *et al.*, 2001) neutron energy distributions in a solid target. This means that those deuterons, which are accelerated inside the dense droplet, are mainly moving along the incident laser axis. This is in clear contrast to the accelerated deuterons from the droplet surface inward; the outward acceleration into  $4\pi$  sr is clearly influenced by the target-droplet geometry.

### 6.2. Spray target

In order to find a promising laser-target concept for efficient fusion neutron production, a methodological approach is

proposed for the comparison of different experimental results. This approach quantifies differences in the target neutron-emission characteristics in relation to the irradiation conditions used (cf. details in Ter-Avetisyan *et al.*, 2005a).

In a deuterium-cluster target irradiated by a high intensity laser, the deuteron ions produced due to the Coulomb explosion were emitted isotropically. Depending on the average density and the geometry of the target, the deuterons, which have sufficient energy for thermonuclear reactions (see Zweiback *et al.*, 2000), can collide with deuterons from nearby clusters and with deuterons inside the clusters in the cold plume. In general, the laser-heated plasma volume is smaller than the cluster plume. The neutron generation volume is determined by the deuterons, which escape the plasma and initiate a D(d,n) reaction within the surrounding cold plume of the jet. Therefore, the neutron generation volume is much larger than the plasma volume. This geometry can be defined as the “beam-target fusion.” The number of neutrons ( $N_n$ ) produced in the cold matter is estimated as

$$N_n \sim N_D \cdot n_D^T \cdot l_T \cdot \langle \sigma_v \rangle, \quad (1)$$

where  $N_D$  is the number of accelerated deuterons, defined as  $N_D = n_D^S \cdot V_S$ ;  $n_D^S$  is the density of the accelerated deuterons;  $V_S$  is the source volume;  $n_D^T$  is the density of target deuterons;  $l_T$  is the path length through the cold plume; and  $\langle \sigma_v \rangle$  is the velocity-averaged fusion cross section as given in Brown and Jarmine (1990).

From Eq. (1), it is obvious that for cluster or gas targets, a huge plasma volume can offset a low fusion cross-section due to a low deuteron kinetic energy and/or low concentration  $n_D^T$  in the target, as shown in Zweiback *et al.* (2000). This will increase the number of accelerated deuterons and the number of fusion neutrons, respectively. As an example, a comparison of the fusion neutron yield from exploding deuterium clusters at different focusing geometries was made in Madison *et al.* (2003), where the estimated difference in the plasma volume by a factor of 10 gave at least a 20 times higher fusion yield. Numerical simulations done in Golovizin and Schep (2003) suggested that the neutron yield might also be increased by shock heating of a large volume during a time longer than the disassembly time of the originally irradiated plasma volume. Furthermore, in various experiments with gas, cluster or spray targets, the value  $l_T$  in Eq. (1) (which is defined by the target jet expansion geometry) is relatively similar, while there are huge differences in the created plasma volumes due to the different focusing geometries used. For all these different conditions, a comparative description has to be found that also includes the interaction geometry. Because the generated energetic deuterons can be measured in absolute terms, and also the number of neutrons created due to deuteron-deuteron collisions is measured directly, we suggest in the following to incorporate the number of accelerated deuterons in a comparison of neutron production from different target

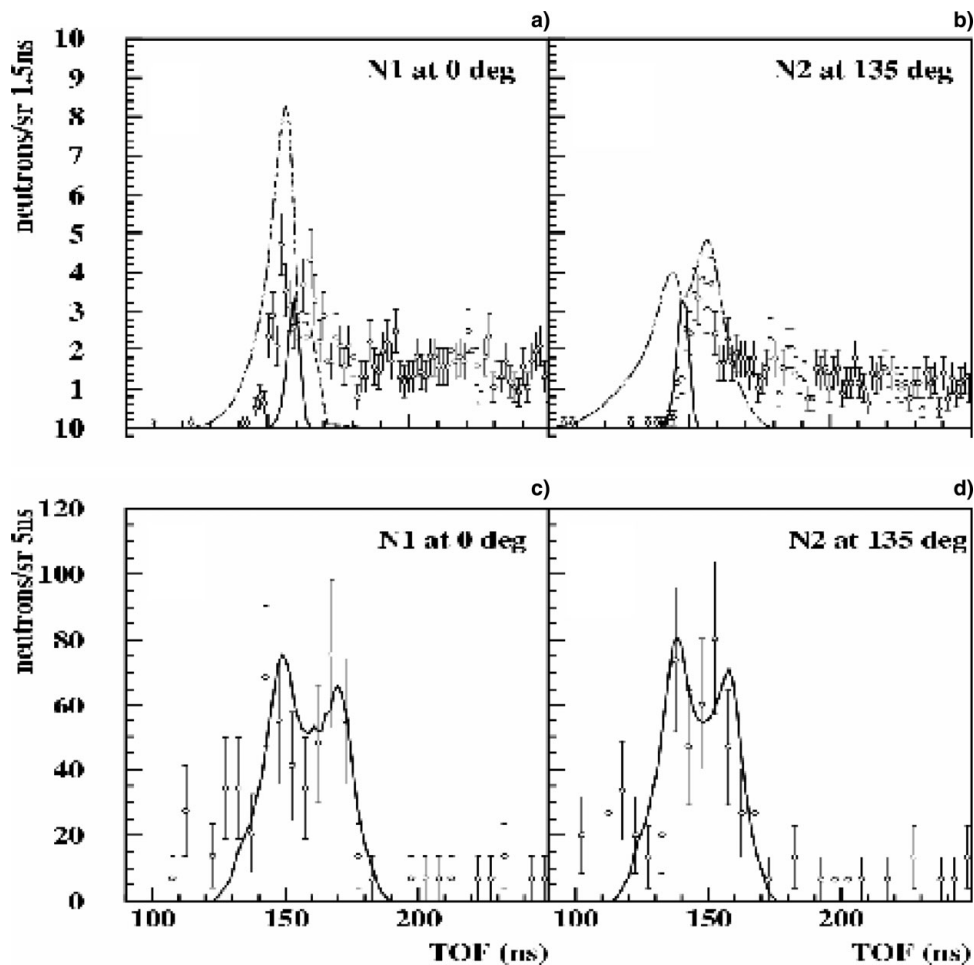


**Fig. 9.** Neutron TOF spectra from the (a), (b) droplet and (c), (d) spray target measured at 0 and 135 degrees to the laser pulse propagation direction, correspondingly. For the droplet target (a), and (b) the neutron yield integrated between 2.0 and 3.0 MeV amounts to 72 and 48 n/sr shot, respectively. The thin solid curve at about 2.45 MeV corresponds to the expected neutron energies from reactions in the neighboring droplets while the dashed line is the result of simulation calculations employing the PIC model (details Schnürer *et al.*, 2004, 2005). The spectral shape of the neutrons from spray target, (c) and (d), is calculated using  $8 \times 10^{10}$  deuterons, which are assumed to be emitted isotropically from the centre of the spray and interacting with a sphere of cold D<sub>2</sub>O. (Sphere radius is 1 mm and the effective areal density is 18  $\mu\text{g}/\text{cm}^2$ ).

systems. Then such an essential geometrical parameter as the plasma volume can be scaled with the number of produced deuterons, and, correspondingly, the number of neutrons.

Therefore, we compare the different target systems by means of the ratio of the number of generated neutrons per accelerated deuteron and incident laser energy or, in other words, the D(d,n) reaction probability per laser pulse energy. The ratio  $N_n/N_D$  is the D(d,n) reaction probability. This includes the efficiency of the energy transfer from the laser to the deuterons, and makes it possible to separate the “plasma volume” effect, when comparing different experiments. Thus an improved characterization of the prospects of a target system for neutron production is possible.

The measured TOF neutron spectra from two neutron detectors positioned at 0° and 135° are displayed in Figures 9c and 9d, respectively. The neutron TOF spectra, calculated (Fig. 2, solid line) with a deuteron spectrum similar to the

measured deuteron emission spectrum, describes well the measurement, assuming a simple model: the produced deuterons collide with a sphere of cold D<sub>2</sub>O matter around the interaction point. The radius of this sphere is 1 mm, and its effective area density is 18  $\mu\text{g}/\text{cm}^2$ . The value is deduced from the average density within the 2 mm extended cloud determined by Ter-Avetisyan *et al.* (2003). Due to the interaction geometry, all D(d,n) reaction angles between 0° and 180° are possible, resulting in high and low energies, respectively, for forward- and backward-emitted neutrons. Employing the measured energy distribution and assuming  $8 \times 10^{10}$  deuterons emitted isotropically into  $4\pi$  sr, the experimental neutron TOF spectra (Figs. 9c, 9d) are reproduced quite well. The values of  $500 \pm 60$  and  $515 \pm 60$  neutrons/sr per pulse are obtained at 0° and 135°, respectively.

From each 0.6 J laser pulse energy,  $6 \times 10^3$  neutrons were produced by about  $10^{11}$  accelerated deuterons (TOF spectra in 0° and 135° is depicted in Figs. 9c and 9d

correspondingly). This corresponds to a D(d,n) reaction probability of about  $6 \times 10^{-8}$ . A comparison to cluster targets, made on the basis of available data shown in Table 1, shows the reaction probability in the spray target to be two orders of magnitude larger. This finding is apparently due to both the considerably higher deuteron energies and the larger effective target thickness in the spray target.

Recently, neutron emission was investigated from a low-density foam target and the ions bulk acceleration mechanism inside the target was demonstrated (Li *et al.*, 2005). The foam and the spray targets have indeed several similarities. The beam target situation of the spray target results in an isotropic emission of neutrons as shown in Figures 9c and 9d, and is similar to those angular positions of Li *et al.* (2005) where the isotropic component is dominant. But of course, the details depend also on the ion energy, and additionally, one would need aerial density of each layer of the foam in order to compare with the droplet size of the spray target. These data from the paper of Li *et al.* (2005) was not possible to extract. First of all and most important, the effective target thickness is three orders of magnitude larger, 5–25 mg/cm<sup>2</sup>, whereas the spray target has only 18 μg/cm<sup>2</sup>. This explains also the huge difference in the number of emitted neutrons per shot.

## 7. STRONG DIPS IN PROTON AND DEUTERON EMISSION SPECTRA

Deep dips in MeV ion spectra are measured from water and heavy water droplet targets of  $\sim 20$  μm diameter irradiated by intense ultrashort (35 fs) laser pulses. It is worth noting that no appreciable isotope effect could be observed. A typical camera picture taken with a single laser shot, showing ion traces from a heavy water droplet, is shown in Figure 10. The deuteron spectrum deduced from this digital CCD-image is shown in the inset. The most interesting features in the picture are the clearly visible dips along the deuteron trace observed in backward (135° to the laser axis) as well as in forward (laser propagation direction) emission. The occurrence of the spectral dips was reproducible in the experiment, although the exact position, depth, and fine

structure varied from shot to shot due to small variations in the laser parameters and beam alignment in our setup (cf. details in Ter-Avetisyan *et al.*, 2003).

The existence of these dips is ascribed to the generation of multi electron-temperature plasma, which is confirmed in our experiments. An existing fluid model (Wickens & Allen, 1981) based on hot-electron components with significantly different temperatures is consistent with the behavior we observe in the ion spectra. The dip in the velocity distribution corresponds to an internal electrostatic sheath appearing due to hot- and cold-electron isothermal expansion, where ions are strongly accelerated in a small region. This dip develops in a region of self-similar flow, where the ions experience a rapid acceleration due to an abrupt increase in the electric field. This increase occurs at the location in the expanding plasma where most of the cold electrons are reflected, corresponding to a step in the ion charge density (See Fig. 6 in Wickens & Allen, 1981). The depth of the dip as a function of the peak field is a sensitive function of the hot-to-cold electron temperature ratio  $T_h/T_c$  in the ion spectra, while the position in the spectrum depends on the hot-to-cold electron density ratio  $n_h/n_c$ .

Figures 11a and 11b compare experimental proton and deuteron energy distributions from single laser shots with calculations based on the theory of Wickens *et al.* (1978). A reasonable fit for the depth and position of the dip in the proton spectrum (Fig. 11a), is obtained when the hot-to-cold electron temperature ratio  $T_h/T_c$  is assumed to be about 9.8, and the hot-to-cold electron density ratio  $n_h/n_c$  is about 1/100. Individual electron temperatures  $T_c = 7.5$  keV and  $T_h = 74$  keV compare quite well to the range of temperatures derived from the X-ray emission measurements, which we performed in the experiments (Ter-Avetisyan *et al.*, 2003). Here,  $T_h$  is lower by a factor of about two, but this can be due to the restricted linearity range ( $< 50$  keV) in the X-ray measurement. Also, if one takes into account that the bulk ion energy scales with the hot electron temperature as  $E_{\text{ion}} = 4.5 T_h$  (Silva *et al.*, 2004), a mean ion energy  $E_{\text{ion}} = 330$  keV would be derived, in a remarkably good agreement with the ion temperature inferred from the ion slope (Fig. 11a). The numerical data fit of high energy tail

**Table 1.** Laser driven fusion neutron sources

Target	Neutron yield (into $4\pi$ )	Laser parameters				D(d,n) Reaction probability/per Joule
		Energy (J)	Duration (fs)	$\lambda$ (nm)	$I_{\text{max}}$ (W/cm <sup>2</sup> )	
D <sub>2</sub> gas <sup>§</sup>	$1 \times 10^6$	62	1000	1.05	$2 \times 10^{19}$	$1.6 \times 10^{-8}$
D <sub>2</sub> O spray*	$6 \times 10^3$	0.6	35	0.8	$1 \times 10^{19}$	$7.5 \times 10^{-8}$
D <sub>2</sub> clusters <sup>§</sup>	$2 \times 10^6$	10	100	0.8	$2 \times 10^{20}$	$5.0 \times 10^{-11}$
CD <sub>4</sub> clusters <sup>&amp;</sup>	$1 \times 10^5$	2.5	100	0.8	$5 \times 10^{19}$	$6.8 \times 10^{-11}$

<sup>§</sup>Fritzler *et al.* (2002).

\*Ter-Avetisyan *et al.* (2005a).

<sup>§</sup>Madison *et al.* (2003).

<sup>&</sup>Madison *et al.* (2004).

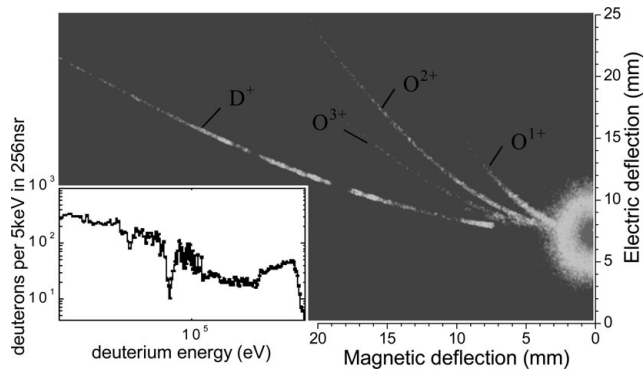


**Fig. 10.** The image from the MCP-phosphorous screen of an emitted ion spectrum (deuterons – most intensive parabolic trace, others – oxygen, right blob – “zero” point: radiation impact along spectrometer axis) from a heavy water droplet taken from a single laser shot in backward ( $135^\circ$  to laser propagation) direction with the Thomson spectrometer. In inset: deuterium spectrum

of the proton spectrum delivers about  $(300 \pm 50)$  keV ion temperature.

Another example of a deuteron energy distribution obtained from a heavy water droplet is presented in Figure 11b, where the cut off energy occurs at about 0.55 MeV. Here the model with a hot-to-cold electron temperature ratio  $T_h/T_c = 7.7$  and an electron density ratio  $n_h/n_c = 1/25$  fits the measurement quite well. The individual temperatures are  $T_c = 11$  keV and  $T_h = 85$  keV. The model shows convincingly how small changes in  $T_e$  and  $n_e$  may have large effects on the spectral shapes.

The model provides a good simulation of the observed spectral dips, and allows us to establish important parameters such as hot- and cold-electron temperatures and the respective electron density ratios.

## 8. QUASI-MONOENERGETIC DEUTERON BURSTS

Here, we report on the generation and laser acceleration of bunches of energetic deuterons with a small energy spread

at maximum energy up to 2 MeV. This quasi-monoenergetic peak within the ion energy spectrum was observed when heavy-water microdroplets were irradiated with ultra-short laser pulses of about 40 fs duration and high ( $10^{-8}$ ) temporal contrast.

The crucial laser parameters of this experiment are the pulse intensity and the contrast ratio, which is the ratio of the prepulse to the pulse peak intensity. In a high-power laser system, each pulse is accompanied by a prepulse of ASE. This low-intensity prepulse might modify the target density profile and affect significantly the interaction of the main ultra short pulse by altering the dynamics of the hot electron population, which, in turn, is responsible for the buildup of the acceleration field at the rear of the target. A high contrast of the laser pulse favors the generation of a large number of hot electrons. The density profile is very steep and the laser energy is thereby efficiently absorbed in a thin skin layer near the solid target surface via Brunel absorption (Brunel, 1987).

In our case, when the ASE level was reduced down to  $10^{-8}$ , the target was transparent for the prepulse, and the main pulse was interacting with an unperturbed target. Then the low energy deuterons gradually disappear and the energy spectrum transforms to a narrow peak as shown in Figure 12a. The selectivity and directionality of the ion acceleration mechanism can be seen from comparison of the deuteron energy spectra in the forward ( $0^\circ$ ) and near-backward ( $135^\circ$ ) directions (Figs. 12b and 12c). The fast ions are moving predominantly in the forward direction, while the backward propagating deuterons have an energy distribution similar to the slow deuterons moving forward. It is interesting to note that the characteristic energy of this slow deuteron component is of the same order as the energies of oxygen ions with charges 2, 3, and 4. The fact that the oxygen ion energy decreases with the ion charge indicates the highly non-stationary ion acceleration process. Very likely the sheath electric field at the rear side of the target is not sufficient for efficient ionization of the oxygen above the charge 2.

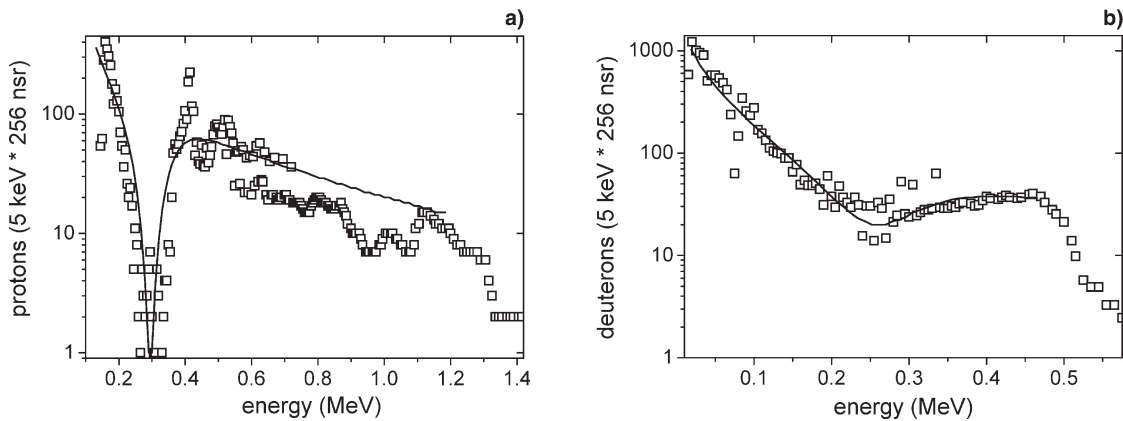


**Fig. 11.** Single shot proton (a) and deuteron (b) spectrum with typical dips along the trace: squares – experiment, line – simulation (parameter cf. text, Sec. 7).

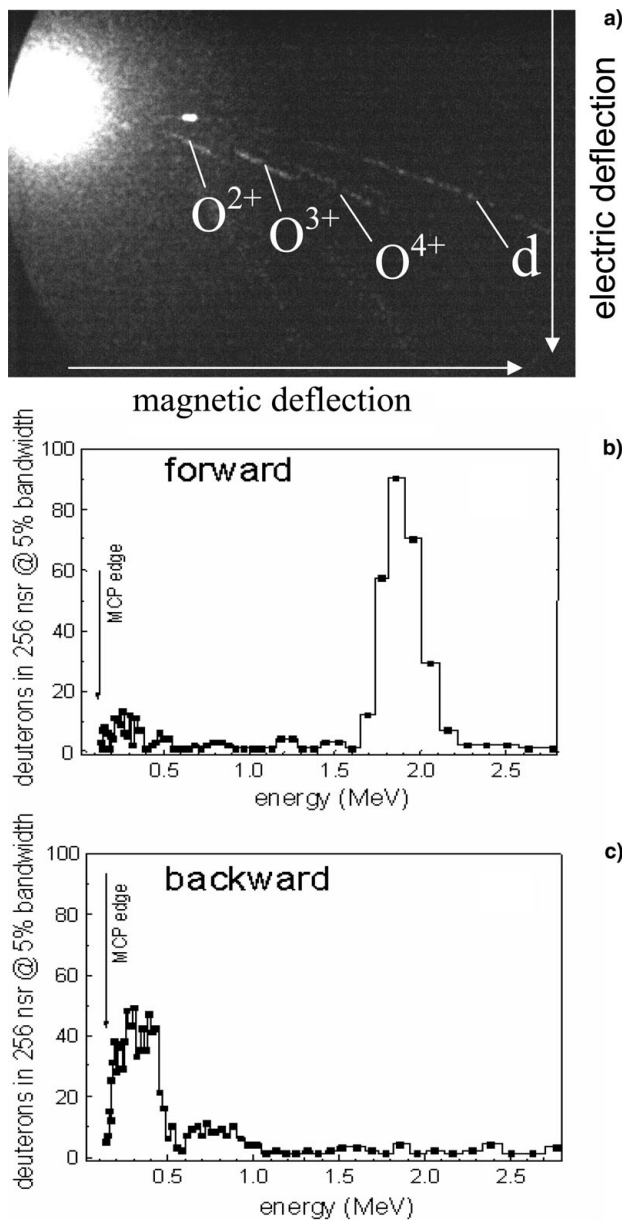


**Fig. 12.** Emitted ion spectra from laser-exposed heavy-water droplets: (a) Thomson-parabola traces of the ion emission (deuterons and oxygen ions) in the forward direction from a heavy water droplet. The color picture shows the dominant deuteron emission in a narrow energy range at high energy. The bright circle in the upper left corner is formed by neutrals and energetic photons are moving along the axis of the spectrometer. (b) Scan of the deuteron energy distribution in the forward direction. (c) Simultaneously emitted deuteron spectra in the backward direction. Here the “monoenergetic” part is left. Only low energy deuterons are visible. The total deuteron energy in the backward direction is less by a factor of two than in the forward direction, whereas their number in the low energy part is higher than in the forward direction.

The ions  $O^{+3}$  and  $O^{+4}$  are created later in time and are less strongly accelerated.

Concerning the narrow energy distribution, two scenarios have been proposed recently. The first one is the heterogenic model (Esirkepov *et al.*, 2002) suggesting that a

thin layer of light ions (protons or deuterons) is deposited on the surface of a target made of heavy ions. It is evident that such a model does not apply to our conditions, where the targets were created *in situ*, and cannot have any contamination layer. This implies that the effect of the narrow deuteron energy spectrum is related to the limited mass of the target combined with a very short pulse excitation.

A model of a homogeneous mixture of light and heavy ions (Tikhonchuk *et al.*, 2005; Gurevich *et al.*, 1972; Allen *et al.*, 2003; Bychenkov *et al.*, 2004; Kemp & Ruhl, 2005) relies on the spatial separation of the light and heavy ions in the electrostatic electric field created by the hot electron population. At a low ASE level, the oxygen ions do not move during the main pulse, and they create the necessary potential jump. All light ions crossing the plasma edge will be accelerated in this potential to the same energy. Therefore, the presence of heavy ions creates the low energy cut off in the energy spectrum of the light ions.

The limited-mass targets have three important advantages. First, they support the planar acceleration geometry only at small distances on the order of the target size; second, they confine the accelerated electrons, which have to rest relatively long time near the target surface allowing the ion acceleration within the target size and prevent their further angular spreading. This is different from the planar geometry, where the fast electrons could be spread along the target surface. The measurements of Cowan *et al.* (2004) and Fuchs *et al.* (2003) reveal the ion emission source size in the foil targets on the order of 50–100  $\mu\text{m}$ , which is five to 10 times larger than the laser focal spot; third, they enable the electrons to access the rear side by passing around the target. Recent calculations suggest that, in addition to the electron pulse propagating through the target, electron currents flow along the spherical surface of the droplet because it is isolated and not grounded. In case of a perfectly symmetrical focusing of the laser pulse at the front target surface, the two electron currents could overlap in time and space at the rear side of the target and strongly enhance the electric field.

The formation of the preplasma deteriorates the deuteron peak formation. The target is surrounded by plasma corona of about the same length as the initial target diameter. Then the divergence of fast electrons is much larger, they spread out and their density and temperature decrease quickly. Evidently this has a negative effect on the sheath electrostatic field.

The essential conclusion is that the short acceleration time combined with a large potential drop forms a quasi-monoenergetic peak-like ion energy distribution. This scenario is also confirmed by the energy spectra of oxygen ions emitted, as are the deuterons, predominantly in the forward direction.

Figure 13 shows some examples of generated monoenergetic bunch of protons together with deuteron spectra of Figure 12a at similar interaction conditions. The latter

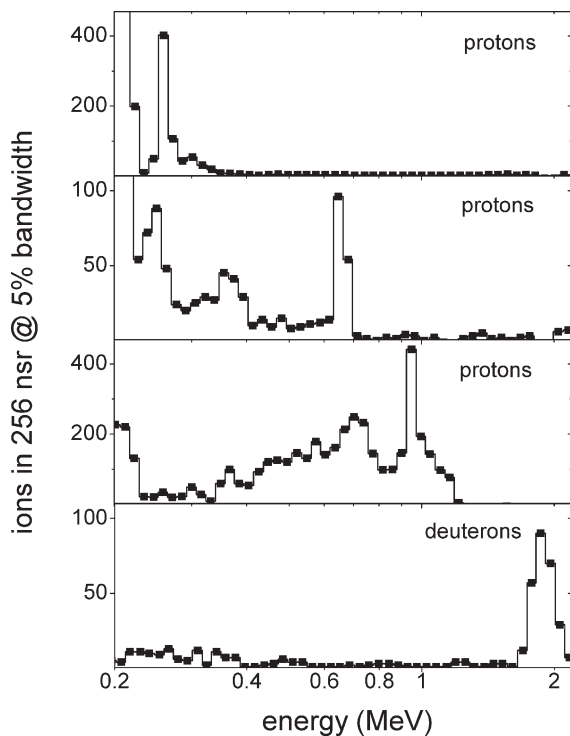


**Fig. 13.** Examples of generated mono-energetic bunches of protons together with deuteron spectra of Fig. 12a) at similar interaction conditions. The latter means that the pulse-to-pulse laser energy fluctuations are within a few percent.

means that the pulse-to-pulse laser energy fluctuations are restricted to a few percent. The observed quite strong variations of the ion peak energy could be attributed to uncontrolled prepulse variations in the time scale of a few ps. Under the condition of a low ASE intensity, these variations may affect strongly the density profile in a sub-micron scale, the efficiency of the laser energy absorption and the electron acceleration. Consequently, the proton/deuteron cut off energies might be extremely sensitive to such laser pulse intensity (or energy) fluctuations. Changes can also be connected with the beam pointing variations on the surface of tiny water droplets. However, it has to be said that the present data allowed us to compare the maximum energies of protons and deuterons emitted from the normal and heavy water droplets. We found that the proton energy is twice smaller than the deuteron energy. This is particularly consistent with the acceleration scenario discussed above, where the velocities of both light ion species, the protons, and the deuterons, are the same.

The theoretical analysis shows that the peak formation in proton/deuteron spectra is fully defined by the level of oxygen ionization at the rear side of the droplet, which is thought to be very sensitive to the laser energy, and the resulting concomitant preplasma level at the front of the droplet. This point could not be resolved from present experimental data. Further development of

the experimental techniques is necessary for an undisturbed detection of the oxygen ionization stages with online controlled all critical experimental parameters in each interaction shot.

## 9. SUMMARY

Recent progress in the study of phenomena in relativistic laser–matter interactions at MBI has been reviewed in this article. Here, we present some final thoughts, conclusions, and hints at plausible future developments.

The developed comprehensive set of on-line ion diagnostics, which are complementary one to another, is a very powerful tool for laser plasma interaction studies. Accessible parameters in the experiments are: the highly resolved ion and electron energy distributions, X-ray emission spectra, highly resolved spatial characteristics of the ion source, temporal evolution of ion emission as well as laser parameters like intensity and contrast. Most of the parameters could be measured simultaneously from a single laser shot.

We would emphasize the importance of use divers diagnostics in each experiment, which only would allow unambiguously demonstrate the ion acceleration processes in their whole complexity, providing a set of data for theoretical interpretation. A complex dynamics of laser-driven ion acceleration for systems ranging from isolated small targets (droplet), clusters (spray), and thin foils were investigated. New and unexpected phenomena have been found: the dips in the ion spectrum, ion emission source characteristics, and distinct absorption mechanism responsible for energy transport and redistribution among the plasma components, etc. Still many challenging effects need to be understood and interpreted, such as nearly “monoenergetic” deuteron and proton bunches from laser-droplet interactions, and the plasma instabilities inside thin foil targets, in particular, in extremely strong Coulomb and laser fields.

We have demonstrated that the laser-plasma ion acceleration has considerable potential as well in terms of active controlling the acceleration processes and tailoring the ion beam. They include ultra short and high contrast laser pulses, potential of different target systems and interaction geometries. It is expected that the near future will be characterized by a significant enhancement of the proton/ion cut off energy, the stable generation of monoenergetic proton/ion beams with low emittance as well as a high efficiency. This will have an impact on many foreseen applications and will encourage further activities for the optimization of laser plasma-based accelerators.

Significant advances in laser technology (Danson *et al.*, 2005; Neumayer *et al.*, 2005) are likely to continue to be achieved for some years to come, hopefully leading to further enhancements in extremely short and high-intensity pulses and a sizeable jump in the achieved power. These developments will surely stimulate the emergence of new ideas and more advanced diagnostic developments for

measuring the effects not even thought of today. All of this is guaranteed to open up new research areas, push currently active ones to new frontiers, and generate further excitement in the field of laser–matter physics.

## ACKNOWLEDGEMENTS

Dedicated to P. V. Nickles in honour his fruitful creative research activities over 40 years, leadership, and friendship at Max Born Institute which will continue to serve as an inspiration to us all. We greatly acknowledge the support in the contrast measurement and the laser operation of M. Kalashnikov and E. Risse. We thank H. Ruhl and A. Kemp for discussions on ion acceleration mechanisms. This work is partly supported by the German Transregio program under TR18 number 6039.

## REFERENCES

- ALBRIGHT, B.J., YIN, L., HEGELICH, B.M., BOWERS, K.J., KWAN, T.J.T. & FERNANDEZ, J.C. (2006). Theory of laser acceleration of light-ion beams from interaction of ultrahigh-intensity lasers with layered targets. *Phys. Rev. Lett.* **97**, 115002.
- ALLEN, M., SENTOKU, Y., AUDEBERT, P., BLAZEVIC, A., COWAN, T., FUCHS, J., GAUTHIER, J.C., GEISSEL, M., HEGELICH, M., KARSCH, S., MORSE, E., PATEL, P.K. & ROTH, M. (2003). Proton spectra from ultraintense laser-plasma interaction with thin foils: Experiments, theory, and simulation. *Phys. Plasmas* **10**, 3283–3289.
- AMMOSOV, M.V., DELONE, N.B. & KRAINOV, V.P. (1986). Tunnel ionization of complex atoms and atomic ions in a varying electromagnetic-field. *Zh. Eksp. Teor. Fiz.* **91**, 2008–2013.
- BORGHESI, M., AUDEBERT, P., BULANOV, S.V., COWAN, T., FUCHS, J., GAUTHIER, J.C., MACKINNON, A.J., PATEL, P.K., PRETZLER, G., ROMAGNANI, L., SCHIAVI, A., TONCIAN, T. & WILLI, O. (2005). High-intensity laser-plasma interaction studies employing laser-driven proton probes. *Laser Part. Beams* **23**, 291–295.
- BORGHESI, M., BULANOV, S., CAMPBELL, D.H., CLARKE, R.J., ESIRKEPOV, T.Z., GALIMBERTI, M., GIZZI, L.A., MACKINNON, A.J., NAUMOVA, N.M., PEGORARO, F., RUHL, H., SCHIAVI, A. & WILLI, O. (2002). Macroscopic evidence of soliton formation in multiterawatt laser-plasma interaction. *Phys. Rev. Lett.* **88**, 135002.
- BORGHESI, M., MACKINNON, A.J., CAMPBELL, D.H., HICKS, D.G., KAR, S., PATEL, P.K., PRICE, D., ROMAGNANI, L., SCHIAVI, A. & WILLI, O. (2004). Multi-MeV proton source investigations in ultraintense laser-foil interactions. *Phys. Rev. Lett.* **92**, 55003.
- BORGHESI, M., SCHIAVI, A., CAMPBELL, D.H., HAINES, M.G., WILLI, O., MACKINNON, A.J., GIZZI, L.A., GALIMBERTI, M., CLARKE, R.J. & RUHL, H. (2001). Proton imaging: A diagnostic for inertial confinement fusion/fast ignitor studies. *Plasma Phys. Control. Fusion* **43**, A267–A276.
- BRAMBRINK, E., ROTH, M., BLAZEVIC, A. & SCHLEGEL, T. (2006a). Modeling of the electrostatic sheath shape on the rear target surface in short-pulse laser-driven proton acceleration. *Laser Part. Beams* **24**, 163–168.
- BRAMBRINK, E., SCHREIBER, J., SCHLEGEL, T., AUDEBERT, P., COBBLE, J., FUCHS, J., HEGELICH, M. & ROTH, M. (2006b). Transverse characteristics of short-pulse laser-produced ion beams: A study of the acceleration dynamics. *Phys. Rev. Lett.* **96**, 154801.
- BROWN, R.E. & JARMIE, N. (1990). Differential cross-sections at low energies for  $^2\text{H}(\text{d},\text{p})\ ^3\text{H}$  and  $^2\text{H}(\text{d},\text{n})\ ^3\text{He}$ . *Phys. Rev. C* **41**, 1391–1400.
- BRUNEL, F. (1987). Not-so-resonant, resonant absorption. *Phys. Rev. Lett.* **59**, 52–55.
- BUSCH, S., SCHNURER, M., KALASHNIKOV, M., SCHONNAGEL, H., STIEL, H., NICKLES, P.V., SANDNER, W., TER-AVETISYAN, S., KARPOV, V. & VOGT, U. (2003). Ion acceleration with ultrafast lasers. *Appl. Phys. Lett.* **82**, 3354–3356.
- BYCHENKOV, V.Y., NOVIKOV, V.N., BATANI, D., TIKHONCHUK, V.T. & BOCHKAREV, S.G. (2004). Ion acceleration in expanding multi-species plasmas. *Phys. Plasmas* **11**, 3242–3250.
- CLARK, E.L., KRUSHELNICK, K., DAVIES, J.R., ZEPF, M., TATARAKIS, M., BEG, F.N., MACHACEK, A., NORREYS, P.A., SANTALA, M.I.K., WATTS, I. & DANGOR, A.E. (2000a). Measurements of energetic proton transport through magnetized plasma from intense laser interactions with solids. *Phys. Rev. Lett.* **84**, 670–673.
- CLARK, E.L., KRUSHELNICK, K., ZEPF, M., BEG, F.N., TATARAKIS, M., MACHACEK, A., SANTALA, M.I.K., WATTS, I., NORREYS, P.A. & DANGOR, A.E. (2000b). Energetic heavy-ion and proton generation from ultraintense laser-plasma interactions with solids. *Phys. Rev. Lett.* **85**, 1654–1657.
- COBBLE, J.A., JOHNSON, R.P., COWAN, T.E., RENARD-LE GALLOUDEC, N. & ALLEN, M. (2002). High resolution laser-driven proton radiography. *J. Appl. Phys.* **92**, 1775–1779.
- COWAN, T.E., FUCHS, J., RUHL, H., KEMP, A., AUDEBERT, P., ROTH, M., STEPHENS, R., BARTON, I., BLAZEVIC, A., BRAMBRINK, E., COBBLE, J., FERNANDEZ, J., GAUTHIER, J.C., GEISSEL, M., HEGELICH, M., KAAE, J., KARSCH, S., LE SAGE, G.P., LETZRING, S., MANCLOSSI, M., MEYRONEINC, S., NEWKIRK, A., PEPIN, H. & RENARD-LEGALLOUDEC, N. (2004). Ultralow emittance, multi-MeV proton beams from a laser virtual-cathode plasma accelerator. *Phys. Rev. Lett.* **92**, 204801.
- DANSON, C.N., BRUMMITT, P.A., CLARKE, R.J., COLLIER, I., FELL, B., FRACKIEWICZ, A.J., HAWKES, S., HERNANDEZ-GOMEZ, C., HOLLIGAN, P., HUTCHINSON, M.H.R., KIDD, A., LESTER, W.J., MUSGRAVE, I.O., NEELY, D., NEVILLE, D.R., NORREYS, P.A., PEPLER, D.A., REASON, C., SHAIKH, W., WINSTONE, T.B., WYATT, R.W.W. & WYBORN, B.E. (2005). Vulcan petawatt: Design, operation and interactions at  $5'10^{20}\text{Wcm}^{-2}$ . *Laser Part. Beams* **23**, 87–93.
- DENAVIT, J. (1992). Absorption of High-Intensity Subpicosecond Lasers on Solid Density Targets. *Phys. Rev. Lett.* **69**, 3052–3055.
- ESIRKEPOV, T.Z., BULANOV, S.V., NISHIHARA, K., TAJIMA, T., PEGORARO, F., KHOROSHKOV, V.S., MIMA, K., DAIDO, H., KATO, Y., KITAGAWA, Y., NAGAI, K. & SAKABE, S. (2002). Proposed double-layer target for the generation of high-quality laser-accelerated ion beams. *Phys. Rev. Lett.* **89**, 175003.
- Fluka-code (2002). <http://www.fluka.org>.
- FRIETZLER, S., NAJMUDIN, Z., MALKA, V., KRUSHELNICK, K., MARLE, C., WALTON, B., WEI, M.S., CLARKE, R.J. & DANGOR, A.E. (2002). Ion heating and thermonuclear neutron production from high-intensity subpicosecond laser pulses interacting with underdense plasmas. *Phys. Rev. Lett.* **89**, 165004.
- FUCHS, J., COWAN, T.E., AUDEBERT, P., RUHL, H., GREMILLE, L., KEMP, A., ALLEN, M., BLAZEVIC, A., GAUTHIER, J.C., GEISSEL, M., HEGELICH, M., KARSCH, S., PARKS, P., ROTH, M., SENTOKU, Y., STEPHENS, R. & CAMPBELL, E.M. (2003). Spatial uniformity of

- laser-accelerated ultrahigh-current mev electron propagation in metals and insulators. *Phys. Rev. Lett.* **91**, 255002.
- FUCHS, J., SENTOKU, Y., KARSCH, S., COBBLE, J., AUDEBERT, P., KEMP, A., NIKROO, A., ANTICI, P., BRAMBRINK, E., BLAZEVIC, A., CAMPBELL, E.M., FERNANDEZ, J.C., GAUTHIER, J.C., GEISSEL, M., HEGELICH, M., PEPIN, H., POPESCU, H., RENARD-LEGALLOUDEC, N., ROTH, M., SCHREIBER, J., STEPHENS, R. & COWAN, T.E. (2005). Comparison of laser ion acceleration from the front and rear surfaces of thin foils. *Phys. Rev. Lett.* **94**, 045004.
- GOLOVIZIN, V.V. & SCHEP, T.J. (2003). Production of direct fusion neutrons during ultra-intense laser-plasma interaction. *J. Phys. D:Appl. Phys.* **31**, 3243.
- GUREVICH, A.V., PARIISKA, L.V. & PITAEVSK, L.P. (1972). Ion acceleration on expansion of a rarefied plasma. *Zh. Eksp. Teor. Fiz.* **63**, 516–531.
- HABARA, H., KODAMA, R., SENTOKU, Y., IZUMI, N., KITAGAWA, Y., TANAKA, K.A., MIMA, K. & YAMANAKA, T. (2003). Momentum distribution of accelerated ions in ultra-intense laser-plasma interactions via neutron spectroscopy. *Phys. Plasmas* **10**, 3712–3716.
- HABS, D., PRETZLER, G., PUKHOV, A. & MEYER-TER-VEHN, J. (2001). Laser acceleration of electrons and ions and intense secondary particle generation. *Prog. Part. Nucl. Phys.* **46**, 375–377.
- HATCHETT, S.P., BROWN, C.G., COWAN, T.E., HENRY, E.A., JOHNSON, J.S., KEY, M.H., KOCH, J.A., LANGDON, A.B., LASINSKI, B.F., LEE, R.W., MACKINNON, A.J., PENNINGTON, D.M., PERRY, M.D., PHILLIPS, T.W., ROTH, M., SANGSTER, T.C., SINGH, M.S., SNAVELY, R.A., STOYER, M.A., WILKS, S.C. & YASUIKE, K. (2000). Electron, photon, and ion beams from the relativistic interaction of petawatt laser pulses with solid targets. *Phys. Plasmas* **7**, 2076–2082.
- HEGELICH, B.M., ALBRIGHT, B.J., COBBLE, J., FLIPPO, K., LETZRING, S., PAFFETT, M., RUHL, H., SCHREIBER, J., SCHULZE, R.K. & FERNANDEZ, J.C. (2006). Laser acceleration of quasi-monoenergetic MeV ion beams. *Nature* **439**, 441–444.
- HEGELICH, M., KARSCH, S., PRETZLER, G., HABS, D., WITTE, K., GUENTHER, W., ALLEN, M., BLAZEVIC, A., FUCHS, J., GAUTHIER, J.C., GEISSEL, M., AUDEBERT, P., COWAN, T. & ROTH, M. (2002). MeV ion jets from short-pulse-laser interaction with thin foils. *Phys. Rev. Lett.* **89**,
- HEMBERG, O., HANSSON, B.A.M., BERGLUND, M. & HERTZ, H.M. (2000). Stability of droplet-target laser-plasma soft X-ray sources. *J. Appl. Phys.* **88**, 5421–5425.
- HILSCHER, D., BERNDT, O., ENKE, M., JAHNKE, U., NICKLES, P.V., RUHL, H. & SANDNER, W. (2001). Neutron energy spectra from the laser-induced  $D(d,n)^3\text{He}$  reaction. *Phys. Rev. E* **64**, 016414.
- KALACHNIKOV, M.P., KARPOV, V., SCHONNAGEL, H. & SANDNER, W. (2002). 100-terawatt titanium-sapphire laser system. *Laser Phys.* **12**, 368–374.
- KALUZA, M., SCHREIBER, J., SANTALA, M.I.K., TSAKIRIS, G.D., EIDMANN, K., MEYER-TER-VEHN, J. & WITTE, K.J. (2004). Influence of the laser prepulse on proton acceleration in thin-foil experiments. *Phys. Rev. Lett.* **93**, 045003.
- KARSCH, S., DUSTERER, S., SCHWOERER, H., EWALD, F., HABS, D., HEGELICH, M., PRETZLER, G., PUKHOV, A., WITTE, K. & SAUERBREY, R. (2003). High-intensity laser induced ion acceleration from heavy-water droplets. *Phys. Rev. Lett.* **91**, 015001.
- KEMP, A.J. & RUHL, H. (2005). Multispecies ion acceleration off laser-irradiated water droplets. *Phys. Plasmas* **12**, 033105.
- KRUEER, W.L. & ESTABROOK, K. (1985). Heating by very intense laser-light. *Phys. Fluids* **28**, 430–432.
- LEFEBVRE, E. & BONNAUD, G. (1997). Nonlinear electron heating in ultrahigh-intensity-laser plasma interaction. *Phys. Rev. E* **55**, 1011–1014.
- LI, Y., SHENG, T.Z.M., MA, Y.Y., JIN, Z., ZHANG, J., CHEN, Z.L., KODAMA, R., MATSUOKA, T., TAMPO, M., TANAKA, K.A., TSUTSUMI, T., YABUCHI, T., DU, K., ZHANG, H.Q., ZHANG, L. & TANG, Y.J. (2005). Demonstration of bulk acceleration of ions in ultraintense laser interactions with low-density foams. *Phys. Rev. E* **72**, 066404.
- LIFSCHITZ, A.F., FAURE, J., GLINEC, Y., MALKA, V. & MORA, P. (2006). Proposed scheme for compact GeV laser plasma accelerator. *Laser Part. Beams* **24**, 255–259.
- MACKINNON, A.J., BORGHESI, M., HATCHETT, S., KEY, M.H., PATEL, P.K., CAMPBELL, H., SCHIAVI, A., SNAVELY, R., WILKS, S.C. & WILLI, O. (2001). Effect of plasma scale length on multi-MeV proton production by intense laser pulses. *Phys. Rev. Lett.* **86**, 1769–1772.
- MADISON, K.W., PATEL, P.K., ALLEN, M., PRICE, D. & DITMIRE, T. (2003). Investigation of fusion yield from exploding deuterium-cluster plasmas produced by 100-TW laser pulses. *J. Opt. Soc. Am. B* **20**, 113–117.
- MADISON, K.W., PATEL, P.K., PRICE, D., EDENS, A., ALLEN, M., COWAN, T.E., ZWEIBACK, J. & DITMIRE, T. (2004). Fusion neutron and ion emission from deuterium and deuterated methane cluster plasmas. *Phys. Plasmas* **11**, 270–277.
- MAKSIMCHUK, A., GU, S., FLIPPO, K., UMSTADTER, D. & BYCHENKOV, V.Y. (2000). Forward ion acceleration in thin films driven by a high-intensity laser. *Phys. Rev. Lett.* **84**, 4108–4111.
- NEUMAYER, P., BOCK, R., BORNEIS, S., BRAMBRINK, E., BRAND, H., CAIRD, J., CAMPBELL, E.M., GAUL, E., GOETTE, S., HAEFNER, C., HAHN, T., HEUCK, H.M., HOFFMANN, D.H.H., JAVORKOVA, D., KLUGE, H.J., KUEHL, T., KUNZER, S., MERZ, T., ONKELS, E., PERRY, M.D., REEMTS, D., ROTH, M., SAMEK, S., SCHAUMANN, G., SCHRADER, F., SEELIG, W., TAUSCHWITZ, A., THIEL, R., URSESCU, D., WIEWIOR, P., WITTRUCK, U. & ZIELBAUER, B. (2005). Status of PHELIX laser and first experiments. *Laser Part. Beams* **23**, 385–389.
- PUKHOV, A. (2001). Three-dimensional simulations of ion acceleration from a foil irradiated by a short-pulse laser. *Phys. Rev. Lett.* **86**, 3562–3565.
- PUKHOV, A., SHENG, Z.M. & MEYER-TER-VEHN, J. (1999). Particle acceleration in relativistic laser channels. *Phys. Plasmas* **6**, 2847–2854.
- SCHNÜRER, M., HILSCHER, D., JAHNKE, U., TER-AVETISYAN, S., BUSCH, S., KALACHNIKOV, M., STIEL, H., NICKLES, P.V. & SANDNER, W. (2004). Explosion characteristics of intense femtosecond-laser-driven water droplets. *Phys. Rev. E* **70**, 056401.
- SCHNÜRER, M., TER-AVETISYAN, S., BUSCH, S., RISSE, E., KALACHNIKOV, M.P., SANDNER, W. & NICKLES, P. (2005). Ion acceleration with ultrafast laser driven water droplets. *Laser Part. Beams* **23**, 337–343.
- SCHREIBER, J., TER-AVETISYAN, S., RISSE, E., KALACHNIKOV, M.P., NICKLES, P.V., SANDNER, W., SCHRAMM, U., HABS, D., WITTE, J. & SCHNÜRER, M. (2006). Pointing of laser-accelerated proton beams. *Phys. Plasmas* **13**, 033111.
- SCHWOERER, H., PFOTENHAUER, S., JACKEL, O., AMTHOR, K.U., LIESFELD, B., ZIEGLER, W., SAUERBREY, R., LEDINGHAM, K.W.D. & ESIRKEPOV, T. (2006). Laser-plasma acceleration of quasi-monoenergetic protons from microstructured targets. *Nature* **439**, 445–448.

- SENTOKU, Y., BYCHENKOV, V.Y., FLIPPO, K., MAKSIMCHUK, A., MIMA, K., MOUROU, G., SHENG, Z.M. & UMSTADTER, D. (2002). High-energy ion generation in interaction of short laser pulse with high-density plasma. *Appl. Phys. B*, **74**, 207–215.
- SENTOKU, Y., COWAN, T.E., KEMP, A. & RUHL, H. (2003). High energy proton acceleration in interaction of short laser pulse with dense plasma target. *Phys. Plasmas* **10**, 2009–2015.
- SHOROKHOV, O. & PUKHOV, A. (2004). Ion acceleration in overdense plasma by short laser pulse. *Laser Part. Beams* **22**, 175–181.
- SILVA, L.O., MARTI, M., DAVIES, J.R., FONSECA, R.A., REN, C., TSUNG, F.S. & MORI, W.B. (2004). Proton shock acceleration in laser-plasma interactions. *Phys. Rev. Lett.* **92**, 015002.
- SNAVELY, R.A., KEY, M.H., HATCHETT, S.P., COWAN, T.E., ROTH, M., PHILLIPS, T.W., STOYER, M.A., HENRY, E.A., SANGSTER, T.C., SINGH, M.S., WILKS, S.C., MACKINNON, A., OFFENBERGER, A., PENNINGTON, D.M., YASUIKE, K., LANGDON, A.B., LASINSKI, B.F., JOHNSON, J., PERRY, M.D. & CAMPBELL, E.M. (2000). Intense high-energy proton beams from petawatt-laser irradiation of solids. *Phys. Rev. Lett.* **85**, 2945–2948.
- STEIN, J., FILL, E., HABS, D., PRETZLER, G. & WITTE, K. (2004). Hot electron diagnostics using X-rays and Cerenkov radiation. *Laser Part. Beams* **22**, 315–321.
- TAJIMA, T. & DAWSON, J.M. (1979). Laser electron-accelerator. *Phys. Rev. Lett.* **43**, 267–270.
- TER-AVETISYAN, S. & NICKLES, P.V. (2006). Ion acceleration at the front and rear surfaces of thin foils with high-intensity 40-fs laser pulses. *JETP Lett.* **83**, 206–210.
- TER-AVETISYAN, S., SCHNURER, M. & NICKLES, P.V. (2005*b*). Time resolved corpuscular diagnostics of plasmas produced with high-intensity femtosecond laser pulses. *J. Phys. D: Appl. Phys.* **38**, 863–867.
- TER-AVETISYAN, S., SCHNURER, M., BUSCH, S., RISSE, E., NICKLES, P.V. & SANDNER, W. (2004). Spectral dips in ion emission emerging from ultrashort laser-driven plasmas. *Phys. Rev. Lett.* **93**, 155006.
- TER-AVETISYAN, S., SCHNURER, M., HILSCHER, D., JAHNKE, U., BUSCH, S., NICKLES, P.V. & SANDNER, W. (2005*a*). Fusion neutron yield from a laser-irradiated heavy-water spray. *Phys. Plasmas* **12**, 012702.
- TER-AVETISYAN, S., SCHNURER, M., NICKLES, P.V., KALASHNIKOV, M., RISSE, E., SOKOLIK, T., SANDNER, W., TIKHONCHUK, V.T. & ANDREEV, A.A. (2006). Quasi monoenergetic deuteron bursts produced by ultraintense laser pulses. *Phys. Rev. Lett.* **96**, 145006.
- TER-AVETISYAN, S., SCHNURER, M., STIEL, H. & NICKLES, P.V. (2003). A high-density sub-micron liquid spray for laser driven radiation sources. *J. Phys. D: Appl. Phys.* **36**, 2421–2426.
- TIKHONCHUK, V.T., ANDREEV, A.A., BOCHKAREV, S.G. & BYCHENKOV, V.Y. (2005). Ion acceleration in short-laser-pulse interaction with solid foils. *Plasma Phys. Control. Fusion* **47**, B869–B877.
- UMSTADTER, D. (2003). Relativistic laser-plasma interactions. *J. Phys. D: Appl. Phys.* **36**, R151–R165.
- WEI, M.S., MANGLES, S.P.D., NAJMUDIN, Z., WALTON, B., GOPAL, A., TATARAKIS, M., DANGOR, A.E., CLARK, E.L., EVANS, R.G., FRITZLER, S., CLARKE, R.J., HERNANDEZ-GOMEZ, C., NEELY, D., MORI, W., TZOUFRAS, M. & KRUSHELNICK, K. (2004). Ion acceleration by collisionless shocks in high-intensity-laser-underdense-plasma interaction. *Phys. Rev. Lett.* **93**, 155003.
- WICKENS, L.M. & ALLEN, J.E. (1981). Ion Emission from Laser-Produced, Multi-Ion Species, 2-Electron Temperature Plasmas. *Phys. Fluids* **24**, 1894–1899.
- WICKENS, L.M., ALLEN, J.E. & RUMSBY, P.T. (1978). Ion emission from laser-produced plasmas with 2 electron temperatures. *Phys. Rev. Lett.* **41**, 243–246.
- WILKS, S.C., KRUER, W.L., TABAK, M. & LANGDON, A.B. (1992). Absorption of ultra-intense laser-pulses. *Phys. Rev. Lett.* **69**, 1383–1386.
- WILKS, S.C., LANGDON, A.B., COWAN, T.E., ROTH, M., SINGH, M., HATCHETT, S., KEY, M.H., PENNINGTON, D., MACKINNON, A. & SNAVELY, R.A. (2001). Energetic proton generation in ultra-intense laser-solid interactions. *Phys. Plasmas* **8**, 542–549.
- YIN, L., ALBRIGHT, B.J., HEGELICH, B.M. & FERNANDEZ, J.C. (2006). GeV laser ion acceleration from ultrathin targets: The laser break-out afterburner. *Laser Part. Beams* **24**, 291–298.
- ZEPF, M., CLARK, E.L., BEG, F.N., CLARKE, R.J., DANGOR, A.E., GOPAL, A., KRUSHELNICK, K., NORREYS, P.A., TATARAKIS, M., WAGNER, U. & WEI, M.S. (2003). Proton acceleration from high-intensity laser interactions with thin foil targets. *Phys. Rev. Lett.* **90**, 064802.
- ZHIDKOV, A., UESAKA, M., SASAKI, A. & DAIDO, H. (2002). Ion acceleration in a solitary wave by an intense picosecond laser pulse. *Phys. Rev. Lett.* **89**, 215002.
- ZWEIBACK, J., SMITH, R.A., COWAN, T.E., HAYS, G., WHARTON, K.B., YANOVSKY, V.P. & DITMIRE, T. (2000). Nuclear fusion driven by Coulomb explosions of large deuterium clusters. *Phys. Rev. Lett.* **84**, 2634–2637.